An engineering approach for estimating the radiation efficiency of orthogonally stiffened plates

Christopher Knuth[1]
Institute of Sound and Vibration Research, University of Southampton
Southampton, SO17 1BJ, UK
C.Knuth@soton.ac.uk

Giacomo Squicciarini
Institute of Sound and Vibration Research, University of Southampton
Southampton, SO17 1BJ, UK
G.Squicciarini@soton.ac.uk

David Thompson
Institute of Sound and Vibration Research, University of Southampton
Southampton, SO17 1BJ, UK
djt@isvr.soton.ac.uk

[1] Corresponding author: C.Knuth@soton.ac.uk.

ABSTRACT

A systematic investigation of the sound radiation of orthogonally stiffened plates is presented using a numerical procedure that combines the finite element method with the Rayleigh integral. Results are computed for stiffened plates with different numbers of stiffeners, stiffener depth, and plate thickness to investigate the dependence on the most important parameters. Differences between the radiation efficiency of stiffened plates and unstiffened panels are seen. In the monopole region, the result depends on the mode that dominates the response. For excitation within a bay, the radiation efficiency is reduced to that of the single bay if the stiffeners are stiff enough. If excited on a stiffener, the plate tends to radiate sound over its full surface area. In the short-circuiting region, on average, the radiation efficiency is equal to that of a smaller bay-sized panel with clamped edges, regardless of the excitation position. Results from the systematic study of 120 numerical cases are used to develop asymptotic formulae for the radiation efficiency of stiffened plates based on existing formulae for unstiffened panels. For all tested configurations, the average difference between the formulae and the numerical calculations was 0.3 dB over the whole frequency spectrum, with a standard deviation of ± 1.5 dB. Between the frequency bands, the mean value varied between -2 and 3 dB, with a standard deviation of up to ± 1.5 dB in the monopole region and up to ± 5 dB in the short-circuiting region.

Keywords: Stiffened plates; sound radiation; radiation efficiency

1. Introduction

Stiffened plates are commonly used in many structures as they can provide a high strength-to-weight ratio. This makes them attractive in aeronautics applications, e.g. in the fuselage of aircraft, but also in civil structures. The stiffeners alter the dynamic properties of the plate and hence its ability to radiate sound [1, 2]. Although stiffened plates have received wide attention in the literature, an easy-to-implement model to estimate their radiation efficiency is still lacking. While for rectangular uniform panels simple analytical expressions for the radiation efficiency are available, to the authors' knowledge an equivalent procedure does not exist for stiffened plates. The development of a new engineering model for estimating the radiation efficiency of stiffened plates is presented in this paper to overcome this gap.

The sound radiation efficiency of a structure can be written as [2]

$$\sigma = \frac{W}{\rho_0 c_0 S \langle \overline{v^2} \rangle} = \frac{R_{\mathrm{rad}}}{\rho_0 c_0 S} \tag{1}$$

where W is the radiated sound power, ρ_0 and c_0 are the density and the speed of sound in air, S is the surface area and $\langle \overline{v^2} \rangle$ is the spatially averaged mean square velocity. The radiation resistance R_{rad} is the ratio of the radiated sound power to the mean-square velocity.

In one of the first investigations of sound radiation from stiffened plates, Maidanik [1] found that these were characterised by a larger radiation resistance than unstiffened panels. He derived asymptotic formulae to predict the radiation efficiency of simply supported unstiffened panels in an infinite rigid baffle, assuming high modal densities. These formulae require knowledge of the material properties, the surface area and the perimeter of the panel and are divided into different frequency regions. Important frequencies delimiting the radiation behaviour are the first panel resonance and the critical frequency, the latter of which can be calculated as [2]

$$f_c = \frac{{c_0}^2}{2\pi}\left(\frac{\mu}{D}\right)^{1/2}, \qquad (2)$$

where μ is the mass per unit area and D the bending stiffness of the plate.

A panel radiates most efficiently around and above its critical frequency, with values of σ exceeding unity. Between the first panel resonance and the critical frequency cancellation due to acoustic short-circuiting occurs; this frequency region can be divided into the ‘corner mode’ and ‘edge mode’ regions [2]. Below its first natural frequency, the panel responds according to its fundamental mode shape and, when mounted in an infinite baffle, radiates sound like a monopole. This frequency range is therefore known as the ‘monopole region’. For stiffened plates, Maidanik suggested that the same formulae could be adopted by increasing the perimeter of the panel by twice the length of the stiffeners. Only a few specific cases were addressed, for which an exact solution was possible.

Comparable results for the radiation resistance of a simply supported panel in a baffle were found by Wallace [3], who evaluated the far-field radiation of single plate modes using the Rayleigh integral [4]. Leppington et al. [5] found that Maidanik’s analysis gave an overestimation around the coincidence region and derived new approximate formulae. The asymptotic formulae from the combined work of [1, 3, 5] are commonly used for the prediction of the radiation efficiency of simply supported panels. They give an estimate of the trend of radiation efficiency over frequency without considering modal behaviour. For simplicity, they will be referred to as Maidanik formulae in this paper. While adapting Maidanik's formulae to plates of very large aspect ratio, Xie et al. [6] demonstrated that the cross-modal contributions can be neglected when considering an average over several excitation positions.

In modelling stiffened plates, narrow stiffeners may be represented by pinned line supports. According to Egle and Sewall [7], this is a suitable assumption if the width of the connection between the stiffener and the plate does not exceed the plate thickness. However, this may not be adequate in a realistic stiffened plate.

In literature, e.g. [8-11], stiffened plates are commonly represented by a system of flexible beams coupled to a plate, which allows for analytical formulations of an idealised stiffened plate. Du et al. [11] investigated the vibration characteristics of stiffened plates for different stiffener placements and plate boundary conditions and verified results by comparison with other models (e.g. Dozio and Ricciardi [8]), and measurements.

Heckl [10] suggested replacing the beam-stiffened plate with an equivalent orthotropic plate unless the distance between adjacent beams is larger than one-quarter of the bending wavelength. In [12], Heckl found pass- and stopband characteristics in periodic arrangements of orthogonally aligned beams. Consequently, wave propagation is possible in distinct frequency regions but highly attenuated in others. Similar behaviour can be expected in a beam-stiffened plate.

Mace [13-15] studied the sound radiation of orthogonally stiffened plates for a point force and the response due to an incident pressure field. Compared with the unstiffened panel, he found an increased far-field sound pressure for a given direction, at frequencies where the acoustic wavenumber coincided with the wave propagation constants of the infinite stiffened plate.

The sound radiation of stiffened plates is addressed by Fahy in [2]. Based on the results of Mead [16], Fahy concluded that Maidanik's results in [1] only roughly describe the actual behaviour of stiffened plates. Further he mentions that treating a stiffened plate as a set of smaller equally-sized panels would be tempting, but requires frequency-dependent boundary conditions.

The finite element method (FEM) allows complex geometries to be modelled, that cannot be solved analytically. Olson and Hazell [17] studied the vibration of orthogonally stiffened plates using the FEM, showing reasonably good agreement compared with measurements. Reynders et al. [18] investigated sound transmission through rib-stiffened plates using the FEM and an equivalent orthotropic plate model. The FE models produced accurate results after adjusting parameters using experimental modal analysis, whereas the orthotropic plate was only acceptable at frequencies corresponding to a few low-order modes. Compared with analytical models, the FEM allows stiffened plates to be modelled more accurately.

Mencik and Gobert [19] used a wave finite element to model the vibration of stiffened plates. They calculated the acoustic radiation of the rectangular plates in an infinite rigid baffle by an elementary source representation.

The aim of this work is to use a systematic set of numerical calculations to provide insight into the radiation efficiency of orthogonally stiffened plates. The results are used to derive a straightforward engineering model to estimate the radiation efficiency of stiffened plates. The asymptotic formulae of Maidanik form the basis of this model and empirical corrections are developed, which combine the influence of important plate and stiffener parameters.

The remainder of the paper is structured as follows. The numerical procedure adopted to calculate the radiation efficiency is presented in Section 2 and the results are shown in Section 3 for different stiffening configurations. In Section 4, the influence of the plate and stiffener stiffness on the radiation efficiency is investigated. In Section 5, the influence of plate boundary conditions is addressed. Empirical corrections to allow the radiation efficiency of stiffened plates to be estimated based on existing engineering formulae are proposed and verified in Section 6.

2. Methodology

In this section, the methodology used to calculate the vibration and radiation efficiency of the stiffened plates is outlined. Numerically calculated modes are combined with the Rayleigh integral to determine the sound radiated by the plate and obtain its radiation efficiency.

2.1. Free Vibration

An FE model of a stiffened plate has been implemented in COMSOL Multiphysics 5.4 to obtain the natural frequencies and mode shapes from a free vibration analysis. The plate and the stiffeners are modelled using shell elements, with the stiffeners connected to one side of the panel. The stiffeners have a C-shaped cross-section, and they are connected to the panel by joining shell elements together. This approach represents the connecting strip between the stiffener and the plate more accurately than a beam model and can include cross-sectional deformation of the stiffener [18]. Clamped boundary conditions are applied to the plate edges, while the stiffener ends are left free. The structure is discretized using triangular elements with a minimum of four second-order elements per structural wavelength [20]. The element size was determined by the highest frequency of observation, which was set to 10 kHz. For consistency between different stiffener configurations, the mode shapes were sampled on a regularly spaced point grid on the plate. An example of the FE model with the mesh and the sampling grid is illustrated in **Fig. 1**.

2.2. Forced vibration

Using the natural frequencies and mode shapes obtained from the FE model, the plate velocity amplitude at the i-th sampling position due to a harmonic point force of circular frequency ω at the k-th forcing position can be calculated using a modal summation [2]

$$v_i = \mathrm{j}\omega \sum_{n=1}^{N} \frac{\psi_{n,i}\psi_{n,k}}{{\omega_n}^2(1+\mathrm{j}\eta)-\omega^2} F_k, \tag{3}$$

where $\mathrm{j} = \sqrt{-1}$ is the imaginary unit, ψ_n the mass-normalized mode shape of the n-th mode at the i-th or k-th sampling position on the plate, ω_n the corresponding natural angular frequency and η the damping loss factor. In the remainder of this paper results are reported for a unit amplitude point force applied to the k-th position ($F_k = 1\ \mathrm{N}$), making the velocity equivalent to the mobility. The force is always assumed to be acting on the side of the plate without stiffeners.

The spatially averaged mean-square velocity of the plate, which is used to calculate its radiation efficiency, is determined by [2]

$$\langle\overline{v^2}\rangle = \frac{1}{ab}\int_S \frac{1}{2}|v(\mathbf{x}_0)|^2 \, \mathrm{d}\mathbf{x}_0, \tag{4}$$

where a and b are the length of the plate in the *x*-direction and *y*-direction, *S* is the surface area of the plate and v is the velocity normal to the plate surface.

2.3. Radiation efficiency

The sound radiation is calculated by assuming that the plate is mounted in an infinite rigid baffle with the radiating side being the one without stiffeners. The sound pressure can be obtained using the Rayleigh integral [4], and discretizing the plate into small equally-sized piston radiators of area $\Delta S = \Delta x \Delta y$ [2]. They are chosen so $\kappa\Delta x < 1$ and $\kappa\Delta y < 1$, where κ is the acoustic wavenumber. The corresponding coordinate system is illustrated in **Fig. 2**.

The sound pressure field can be calculated as [2]

$$\mathbf{p}(\mathbf{x}) = \mathbf{Z}(\mathbf{x}_0|\mathbf{x})\mathbf{v}(\mathbf{x}_0), \tag{5}$$

where $\mathbf{p}$ contains the pressures at all acoustic field points, $\mathbf{v}$ the normal plate velocities obtained from the sampling grid of the FE model and $\mathbf{Z}$ is an impedance matrix of terms that link the plate velocities at $\mathbf{x}_0$ to the sound pressures at $\mathbf{x}$. The impedance term that links the i-th elemental source with the j-th receiver is defined as [2]

$$Z_{ij}(\omega) = \mathrm{j}\omega\rho_0 \frac{e^{-\mathrm{j}\kappa R_{ij}}}{2\pi R_{ij}} \Delta S_i, \tag{6}$$

where ρ_0 is the density of air, R_{ij} is the distance between the i-th and j-th element, and ΔS_i is the surface area of the i-th element of the plate.

The acoustic power is approximated by a discrete integration of the far-field intensity over the small surface elements associated with each receiver as [2]

$$W = \sum_{j=1}^{J} \frac{|p_j|^2}{2\rho_0 c_0} \Delta S_j, \tag{7}$$

where ΔS_j is the surface area of the j-th receiver, with $\Delta S_j = r_j^2 \sin\theta_j \, \Delta\theta_j \Delta\phi_j$ on a hemisphere.

Finally, the radiation efficiency of the plate can be obtained from Eq.(1). The spatially averaged radiation efficiency is calculated as [21]

$$\overline{\sigma} = \frac{\overline{W}}{\rho_0 c_0 ab \overline{\langle \overline{v^2} \rangle}}, \tag{8}$$

where $\overline{\langle \overline{v^2} \rangle}$ and $\overline{W}$ indicate an average over various forcing positions.

2.4. Parametric study

Stiffened plates are considered here with a regular stiffener spacing. The center line of the stiffeners is aligned at an equal distance and all C-shaped stiffeners are oriented in the same direction. Due to the non-centered web that connects the two flanges, the stiffened plate is not symmetric. The stiffeners divide the panel into smaller sections, or 'bays'.

Four different stiffening configurations are studied, with increasing numbers of stiffeners, as shown in **Fig. 3**. They will be referred to as 'Cases'. For each of the cases, three different plate thicknesses and ten stiffener depths are considered, while maintaining the plate surface area. In total, therefore, 120 configurations of stiffened plates are studied. Twenty forcing positions are used, distributed in the bay regions and on the stiffeners, to obtain average radiation efficiencies. As the topography of the plate varies for each case, the forcing positions were adjusted to keep similar numbers of positions on the stiffeners and in the bays in each case. The parameters adopted in the numerical studies are listed in **Table 1**.

3. Sound radiation for different numbers of stiffeners

The effect of the number of stiffeners attached to a thin plate on its radiation efficiency is first evaluated for different forcing positions. The depth of the stiffeners is set to 40 mm in this section, and a relatively thin plate of 1.5 mm thickness is used to emphasise the effect of adding the stiffeners.

For each case, the average radiation efficiencies are obtained by averaging over the forcing positions on the bays and stiffeners separately, as marked in **Fig. 3**. These two excitation configurations are analysed separately, as the frequency response (not shown here) showed significant differences in magnitude and number of resonances in the response depending on the position of the forcing points. The low-order modes of stiffened plates occur in clusters with several modes in a narrow frequency range, but their contribution to the response depends largely on whether the forcing point is on a stiffener or in a bay between stiffeners. As an example, the radiation efficiencies of

Case 3 are presented in **Fig. 4** (in the form of radiation index $L_\sigma = 10\log_{10}\sigma$). They are compared with the unstiffened panel and a smaller panel of size equal to a single bay with clamped edges.

In the low-frequency monopole region, the radiation efficiencies rise at 20 dB/decade $(\sim f^2)$ up to the frequency of the fundamental mode. This natural frequency is increased from around 30 Hz for the unstiffened panel to 260 Hz in the presence of the stiffeners. In the monopole region, the stiffener-excited plate follows the trend of the unstiffened panel, whereas radiation efficiency is lower and close to the bay-sized unstiffened panel when excited in the bays. This behaviour is a consequence of the mode type that dominates the low-frequency response. In the case of bay excitation, a "plate-dominated" mode responds, where the stiffeners remain mostly rigid and restrict the motion to the excited bay. For stiffener excitation, a "stiffener-dominated" mode determines the response, with the stiffeners imposing displacement over the whole plate. The response shapes for the unstiffened panel and stiffened plate are added in **Fig. 4** for a single excitation position on a stiffener and in a bay to highlight this behaviour.

In the short-circuiting region, the radiation efficiency of the stiffened plate is similar for both forcing locations and agrees closely with that of the smaller clamped panel with the size of a single bay. Due to the stiffeners, the bays radiate sound more independently in this frequency region. Above the critical frequency (8 kHz for this thickness) all the results converge towards unity or 0 dB.

The results of Cases 1-4 are presented in **Fig. 5**. They are shown in a one-third octave band frequency resolution to allow differences to be seen more clearly. Although the general trends are similar to those seen in **Fig. 4**, there are substantial differences between the radiation due to bay excitation in **Fig. 5**(a) and stiffener excitation in **Fig. 5**(b), particularly at low frequency.

For bay excitation, **Fig. 5**(a), as the number of stiffeners is increased, the monopole region extends to higher frequencies due to the higher fundamental natural frequency. Moreover, the radiation efficiency in this region is reduced in proportion to the ratio of bay-to-plate surface areas S_{bay}/S. This is demonstrated in **Table 2**, where the reduction in the monopole region at the example frequency of 10 Hz is estimated correctly within $\pm$0.5 dB by the ratio S_{bay}/S. In the short-circuiting region, the radiation efficiency increases if the bay surface area is reduced. This is also demonstrated at an example frequency of 2 kHz in **Table 2**. However, the radiation efficiency can vary strongly within the short-circuiting region due to the modal dips and peaks. Above the critical frequency, the radiation efficiency of all the plates becomes similar to that of the unstiffened panel.

For stiffener excitation, **Fig. 5**(b), the radiation efficiency in the monopole region is roughly equal to that of the unstiffened panel but the monopole-like behaviour again extends up to higher frequencies. In the short-circuiting region, the results are almost identical to those found for bay excitation.

The results show changes in the radiation efficiency of stiffened plates compared with an unstiffened panel of the same thickness. The excitation position determines the low-frequency radiation of sound, which can be decreased to that of a monopole having the size of a single bay only for excitation in a bay. At higher frequencies, the radiation efficiency increases as the bay size decreases.

4. Effect of plate and stiffener flexibility on the radiation efficiency

The role of the plate thickness and stiffener depth, which define their respective bending stiffness, is analysed in this section. The stiffened plate of Case 3 is first used to assess both effects for some example configurations. Thereafter, the results of all 120 configurations are summarised in non-dimensional form.

4.1. Effect of plate thickness

The effect of the plate bending stiffness on the radiation efficiency is investigated by increasing the thickness from 1.5 to 3 and 6 mm in the FE model, while keeping the stiffener depth at 40 mm. The calculations are also performed for unstiffened panels of the same thicknesses.

The radiation efficiencies of the 3 mm and 6 mm stiffened plates and unstiffened panels are shown in **Fig. 6**; the 1.5 mm plate of Case 3 can be found in **Fig. 5**. In the monopole region, both stiffened plates have the same radiation efficiency as the unstiffened panel when excited on a stiffener. Considering excitation in the bays, the radiation efficiency in the monopole region is significantly affected by the plate thickness. The 3 mm plate is reduced by around 5 dB compared with the unstiffened plate of the same thickness, while the 6 mm plate radiates almost unreduced. In the case of the 1.5 mm plate, the reduction was 9-10 dB, i.e. the radiating surface corresponded to that of the bay. The low-frequency response of the thicker stiffened plates is dominated by a fundamental mode, where almost the whole plate vibrates, like an orthotropic plate. With increasing plate thickness, the vibration is less constrained by the stiffeners. Hence, a surface area larger than the forced bay can radiate sound, which explains the lesser reduction for bay excitation.

In the short-circuiting region, an increase in radiation efficiency can be seen compared with the unstiffened panel and it is again similar for excitation in the bay and on the stiffener. The critical frequency of the 3 mm plates is around 4 kHz and for the 6 mm near 2 kHz. The radiation efficiency of the 6 mm plate reaches unity (0 dB) already below the critical frequency, due to the extended monopole region. Above coincidence, the differences with the unstiffened panel vanish in each case.

4.2. Effect of stiffener depth

The effect of the stiffener flexibility on the radiation efficiency of the stiffened plate is shown by comparing the radiation efficiency with stiffener depths h_s between 20 and 100 mm for Case 3 with a plate thickness of 3 mm.

The results are shown in **Fig. 7**(a) for bay excitation. With increasing stiffener depth, the radiation efficiency decreases in the monopole region, as the vibration becomes increasingly constrained by the stiffeners, until it is restricted to a single bay. This is analogous to the effect of reduced plate thickness for a constant stiffener depth, as discussed in Section 4.1. For $h_s > 60$ mm, the monopole-like trend of the radiation efficiency extends beyond the first natural frequency. The first few modes of these plates have lower natural frequencies than the other plates with $h_s \leq 60$ mm and are associated almost entirely with the deformation of the stiffeners, which does not induce significant motion on the surrounding bays. The dip around 400 Hz for $h_s = 100$ mm corresponds to a cluster of such stiffener-dominated modes. The short-circuiting region effectively starts at the frequency of the first mode that principally involves vibration in the plate. For $h_s = 100$ mm, this occurs above the 630 Hz band. Above 1 kHz, the results converge to similar values, irrespective of the stiffener depth, owing to the higher-order plate-dominated modes of the stiffened plate, which has the same thickness and bay dimensions in the presented cases.

For stiffener excitation, **Fig. 7**(b), the main differences from bay excitation are visible below the fundamental mode. For $h_s \leq 60$ mm, the plates radiate as efficiently as the unstiffened panel in the monopole region, as already shown in **Fig. 5** and **Fig. 6**. For deeper stiffeners, in the studied cases for $h_s >$ 60 mm, the radiation efficiency is reduced from the unstiffened panel result. This occurs because higher-order modes contribute significantly to the low-frequency response and the net sound radiation decreases from the monopole efficiency, due to some cancellation effects. The reduction is case-dependent but more pronounced for thinner plates, where the stiffeners are relatively stiff compared with the plate.

4.3. The difference in the monopole region

The results in Sections 4.1 and 4.2 showed that changes in plate thickness or stiffener depth have a large impact on the monopole region. This region extends to higher frequencies for stiffened plates and can therefore be of more relevance than for unstiffened panels.

To analyse this phenomenon, the ratio of the radiation efficiencies σ/σ_0 between the stiffened (σ) and unstiffened plates (σ_0) was averaged over frequency bands below the first mode. The results of Cases 1 and 4 are shown in **Fig. 8** for different plate thicknesses and stiffener depths. The horizontal axis represents the ratio EI_b/D of the stiffener (EI_b) to the plate (D) bending stiffness on a logarithmic scale. For bay excitation, the results form two distinct groups according to the case considered. At large values of EI_b/D, the results reduce to -6 dB for Case 1 and -10 dB for Case 4. This corresponds approximately to $10\log_{10}(S_{\mathrm{bay}}/S)$. For the stiffener excitation, the results initially increase marginally with increasing EI_b/D and then they start to drop at different values of EI_b/D, causing a larger spread of the data. A misalignment between the cases can be seen, which suggests that the ratios σ/σ_0 and EI_b/D do not sufficiently capture the overall trends.

To align the results vertically, a non-dimensional parameter γ is established based on the ratio σ/σ_0. **Table 2** and **Fig. 8** showed that the maximum expected reduction of radiation efficiency is equal to the ratio of the plate-to-bay surface areas. Therefore, γ is defined as

$$\gamma = \frac{10\log_{10}(\sigma/\sigma_0)}{10\log_{10}\left(S/S_{\mathrm{bay}}\right)}, \tag{9}$$

which has a value of $\gamma = 0$ for $\sigma = \sigma_0$ and $\gamma = -1$ for $\sigma/\sigma_0 = S_{\mathrm{bay}}/S$.

To align the results horizontally, the ratio EI_b/D (which has units of metres) is normalised by the total length of all stiffeners. For bay excitation, a better representation is found when further normalising by the number of bays. This results in two additional non-dimensional parameters, β for bay excitation and $\hat{\beta}$ for stiffener excitation, defined as

$$\beta = \log_{10}\left(\frac{EI_b}{D\ L_s N_{\mathrm{bay}}}\right), \tag{10}$$

$$\hat{\beta} = \log_{10}\left(\frac{EI_b}{D\ L_s}\right), \tag{11}$$

where L_s is the total length of all stiffeners and N_{bay} the number of bays.

The results from all 120 cases are summarized in this non-dimensional form in **Fig. 9**. Compared with **Fig. 8**, a smaller spread of the data can be seen. A value of $\gamma = 0$ indicates that the radiation efficiency equals that of the unstiffened panel, while for $\gamma = -1$ it corresponds to that of a bay-sized panel. Positive values are possible and denote an increase compared with the unstiffened panel. For example, a change of γ by ± 0.2 corresponds to a change in radiation efficiency of approximately ± 1 dB for Case 1 (largest bay size) and ± 2 dB for Case 4 (smallest bay size).

For bay excitation, **Fig. 9**(a), all the results merge into an inverted S-shaped curve which can be broadly divided into three regions of β. The data can be approximated by an asymptotic function that consists of two constants and a linear function of the normalised bending stiffness ratio β. From curve fitting it is obtained as

$$\gamma_{\mathrm{fit},1} = \begin{cases} 0 & \text{for } \beta < -0.52, \\ -0.60\beta - 0.31 & \text{for } -0.52 \le \beta \le 1.14, \\ -1 & \text{for } \beta > 1.14. \end{cases} \tag{12}$$

The first region extends up to $\beta < -0.52$ with $\gamma \approx 0$. It includes cases with thick plates and relatively shallow stiffeners, where the plates tend to vibrate over their full surface area due to stiffener-dominated modes. The second region, between $\beta \geq$

-0.52 and $\beta \leq 1.14$, corresponds to a transition of the low-frequency behaviour from stiffener-dominated to plate-dominated fundamental modes. Thus, γ decreases gradually with increasing β. Both regions are well represented by Eq. (12). In the third region where $\beta > 1.14$, the stiffeners are stiff enough to constrain the plate motion and cause the first modes to be plate-dominated. Hence, the radiation efficiency is equivalent to, or lower than, that of a single bay. Although the constant $\gamma = -1$ adopted in Eq. (12) deviates from the data, it is preferred here to give the physical limitation of a single vibrating bay. The reduction is due to complex vibration patterns arising from the interaction between the deep stiffeners and the thin plate. The expected error is in the range of 1-3 dB for the four cases analysed.

For stiffener excitation, **Fig. 9**(b), the curve has a different shape and can be divided into two regions of $\hat{\beta}$. To approximate the numerical data, an asymptotic function that consists of two linear curves has been obtained from curve fitting as

$$\gamma_{\mathrm{fit},2} = \begin{cases} 0.01\hat{\beta} + 0.08 & \text{for } \hat{\beta} \leq 1.80, \\ -0.64\hat{\beta} + 1.25 & \text{for } \hat{\beta} > 1.80. \end{cases} \tag{13}$$

Up to $\hat{\beta} \approx 1.8$, γ increases slightly with increasing stiffness ratio, whereas there is a decreasing trend starting from about $\hat{\beta} > 1.8$. This range includes cases with very stiff stiffeners on a rather flexible plate. Although all the cases analysed present a general decreasing trend with increasing $\hat{\beta}$ in this range, the scatter is high. The plate configurations with $\hat{\beta} \gg 1.8$ are assumed to be rather extreme, and a common behaviour is not found. Stiffened plates belonging to this region may need to be studied on a case-by-case basis.

In summary, changing either the thickness of the plate or the depth of the stiffeners alters the low-frequency sound radiation of the stiffened plates. The more constrained is the vibration of the plate, the smaller its radiating monopole surface area. The radiation efficiency decreases from that of a plate vibrating over its whole surface area roughly to that of a single bay, a trend that is found to be proportional to the ratio of stiffener-to-plate bending stiffness.

5. Effect of structural boundary conditions

Further numerical calculations are presented in this section to demonstrate the influence of the boundary conditions at the plate edges on the radiation efficiency of stiffened plates. Some of the calculations initially performed with clamped edges are repeated with simply supported edges. In support of this discussion and to introduce approximations for the radiation efficiency of stiffened plates, the results obtained with the Maidanik formulae, see Eq. (18a-d) in Appendix A, are used for comparison.

The results of **Fig. 4** indicate that a clamped bay-sized panel may offer a more suitable approximation for the radiation of stiffened plates in the short-circuiting region. It is therefore necessary to adapt Maidanik's formulae to the case of clamped edges. This procedure is presented in Appendix A. To account for clamped edges, the monopole region of Eq. (18a-d) is replaced with Eq. (19), and short-circuiting region with Eq.(20).

In **Fig. 10**, the radiation efficiencies of two stiffened plates with either clamped or simply supported boundaries are shown for bay excitation; the stiffening configurations correspond to cases with $\beta = -0.47$ in (a) and $\beta = 1.28$ in (b). Results from the Maidanik formulae for a simply supported panel and a clamped panel are added for comparison, using the fundamental natural frequency f_1 of the stiffened plates and reducing the plate surface area and perimeter to that of a single bay for both regions $f < f_1$ and $f_1 < f < f_c$. Different observations can be made about the behaviour in the monopole and short-circuiting regions.

In the monopole region, for configurations with $\gamma \approx 0$, the stiffened plates tend to vibrate over their full surface area, and the boundary conditions at the outer edges can result in different radiation ratios. This can be seen in **Fig. 10**(a), where the simply supported stiffened plate has a higher radiation efficiency than the clamped one. The difference is only about 1 dB, which agrees with the results for unstiffened panels in [21]. This result holds irrespective of the forcing position; an equivalent result was found for excitation on the stiffeners. The approximation with the bay-sized panels does not work in this frequency range. The results for the bay-sized panels jump at 250 Hz because the monopole region is delimited by f_1 of the stiffened plates.

For the configurations characterised by $\gamma \approx -1$, for example **Fig. 10**(b), the boundary conditions at the plate edges have a less important role in the monopole region. In these cases, the vibration is confined within the single bays and the radiation efficiency of the whole plate is well represented by bay-sized panels. The simply supported bay-sized panel would slightly overestimate the result for the stiffened plate in the monopole region, suggesting the stiffeners add conditions to the bay that are rather clamped-like.

In both plates considered in **Fig. 10**, the efficiency in the short-circuiting region remains similar for simply supported and clamped edges. In the corner mode region, below 1 kHz where the radiation efficiency on average remains flat, the simply supported bay-sized panel underestimates the stiffened plate result, while the clamped panel gives on average a good estimation. In the edge mode region above 1 kHz, where efficiency increases as frequency approaches the critical frequency, the clamped panel also provides the better approximation. Around the coincidence, both bay-sized panels converge to the same value.

In conclusion, a simply supported bay-sized panel is not well suited to approximate the stiffened plate in the short-circuiting region, and a better solution is found using clamped boundaries. The monopole region needs a correction that accounts for the decrease of the radiating surface area of the plate, which is not in all cases as simple as reducing it to the bay-sized panel.

6. Engineering formulae for radiation efficiency

Similar trends were found for the radiation efficiency of stiffened plates and unstiffened panels. This allows the Maidanik formulae for unstiffened panels to be used and adapted for the stiffened plates. Empirical corrections based on the results from the previous sections are combined with the Maidanik formulae. The extended formulae are tested over a wide range of configurations to establish the applicability of the predictions.

6.1. Correction in the monopole region

Considering the monopole region ($f < f_1$), for bay excitation the trend of the radiation efficiency shown in **Fig. 9**(a) can be approximated by Eq. (12) and for stiffener excitation with Eq. (13), see **Fig. 9**(b). The values of the fitted asymptotic function γ_{fit} can be used to derive a correction for the monopole region if stiffeners are added to the plate.

Re-arranging Eq. (9) and using $\gamma_{\mathrm{fit},i}$ from either Eq. (12) or Eq. (13), the change in radiation ratio due to the introduction of stiffeners can be expressed as

$$\Delta L_\sigma = 10\log_{10}(\sigma/\sigma_0) = \gamma_{\mathrm{fit},i}\, 10\log_{10}\left(S/S_{\mathrm{bay}}\right). \tag{14}$$

Hence, the radiation efficiency of stiffened plates in the monopole region becomes

$$\sigma = \frac{\varepsilon f^2 S}{{c_0}^2}\left(\frac{S_{\mathrm{bay}}}{S}\right)^{-\gamma_{\mathrm{fit},i}}, \tag{15}$$

where i indicates that the excitation is either within the bays ($i = 1$) or on the stiffeners ($i = 2$) and an additional factor ε is added to account for the boundary conditions on the plate edges. If $\gamma_{\mathrm{fit}} = 0$, the monopole radiation efficiency is calculated for a plate radiating over its whole surface area, and for $\gamma_{\mathrm{fit}} = -1$ the area of a single bay is used. For simply supported plate edges, if $\gamma_{\mathrm{fit}} \approx 0$, the value $\varepsilon = 4$ should be used. Otherwise, $\varepsilon = 3$ of the clamped panel is more appropriate. However, the difference in radiation ratio between $\varepsilon = 3$ and $\varepsilon = 4$ is only about 1.3 dB. This is usually small compared with ΔL_σ and of lesser importance if the correct boundary condition of the bay edges is uncertain.

6.2. Correction in the short-circuiting region

A correction to account for the increase of the radiation efficiency in the short-circuiting region ($f_1 < f < f_c$) due to the presence of stiffeners is presented here. The results from Sections 3-5 showed that, irrespective of the excitation position, the radiation efficiency of the stiffened plate is increased when decreasing the bay size. On average, regardless of the boundary conditions at the plate edges, the radiation efficiency in the short-circuiting region was found to be reasonably well approximated by that of a bay-sized panel with clamped edges. Thus, the radiation efficiency in the short-circuiting region can be calculated by

$$\sigma = \max\left(\frac{8\pi^2}{{c_0}^2 S_{\mathrm{bay}}}\frac{D}{\mu}, \frac{X P_{\mathrm{bay}}}{4\pi^2 S_{\mathrm{bay}} f_c}\frac{(1-\alpha^2)\ln\left(\frac{1+\alpha}{1-\alpha}\right)+2\alpha}{(1-\alpha^2)^{3/2}}\right), \tag{16}$$

where P_{bay} is the perimeter of a single bay, S_{bay} is its surface area and the factor of X is introduced in Eq. (21) in Appendix A to account for the radiation efficiency of clamped edges in the edge mode region, while in the corner mode region the factor of 2 is applied.

6.3. Accuracy of the prediction based on proposed corrections

In this section, the extended Maidanik formulae with the corrections derived in Sections 6.1 and 6.2 are tested against the more exact numerical calculations. In summary, the extended asymptotic formulae to estimate the radiation efficiency of orthogonally stiffened plates are given as

$$\sigma = \begin{cases} \dfrac{\varepsilon f^2 S}{{c_0}^2}\left(\dfrac{S_{\mathrm{bay}}}{S}\right)^{-\gamma_{\mathrm{fit}}} & \text{for } f < f_1, \\ \max\left(\dfrac{8\pi^2}{{c_0}^2 S_{\mathrm{bay}}}\dfrac{D}{\mu}, \dfrac{XP_{\mathrm{bay}}}{4\pi^2 S_{\mathrm{bay}} f_c}\dfrac{(1-\alpha^2)\ln\left(\dfrac{1+\alpha}{1-\alpha}\right)+2\alpha}{(1-\alpha^2)^{3/2}}\right) & \text{for } f_1 < f < f_c\,, \\ 0.45\sqrt{\dfrac{Pf_c}{c_0}}\left(\dfrac{b}{a}\right)^{1/4} & \text{for } f \approx f_c\,, \\ \left(1-\dfrac{f_c}{f}\right)^{-1/2} & \text{for } f > f_c. \end{cases} \quad \text{(17a-d)}$$

They apply to stiffened plates with clamped or simply supported boundaries and allow predictions at a much lower computational cost than the full numerical procedure. The delimiting value of f_1 needs to be obtained from an FE or analytical model of the stiffened plate. In the monopole region, the value of γ_{fit} is based on Eq. (12) for bay excitation and Eq. (13) for stiffener excitation. In the short-circuiting region, the increase relative to the simply supported unstiffened panel is accounted for by the factor X, see Eq. (21). The coincidence region and above were not adjusted.

The level differences in decibels between the results obtained from Eq. (17a-d) and the numerical models are determined for the 120 configurations in each one-third octave band. Over all 120 cases and all the frequency bands the average error has a mean value of 0.3 dB with a standard deviation of $\pm$1.5 dB, while in single frequency bands the mean value ranges from $-$0.3 and 1.1 dB and the standard deviation can be as large as $\pm$3.5 dB. The engineering model of stiffened plates in Eq. (17a-d) tends to overestimate the radiation efficiency slightly on average.

There are differences in the average error when the results are separated for different plate thicknesses; this avoids overlapping the frequency regions below and above coincidence. In **Fig. 11** the error is shown as the mean values and a range of +/- one standard deviation per frequency band, separately for bay and stiffener excitation. The minimum and maximum differences are also shown. Positive values denote an overestimation compared with the numerical results.

Below 80 Hz, where the stiffened plates radiate as monopoles, the average error lies within a band of ±2 dB for each of the three different thicknesses. The standard deviation is largest for the 1.5 mm plates for stiffener excitation, due to the larger scatter of γ in the region with $\hat{\beta} > 1.8$, where many of these plates lie. For the 3 and 6 mm plates the standard deviation is closer to ±1 dB.

Between 80 Hz and 400 Hz, the stiffened plates have a transition from the monopole to the short-circuiting region. Some plates are still radiating like monopoles, while others are already in the short-circuiting region, where the error increases. In the short-circuiting region, the mean value of the error lies between -2 and 3 dB. The standard deviation varies for the three plate thicknesses and can be as high as ±5 in case of the 1.5 mm plate. For the 3 and 6 mm plates it decreases to about ±4 and ±3 dB respectively. The errors in this region are similar for bay and stiffener excitation. A maximum error of 10-15 dB can be found in some frequency bands due to the modal behaviour of the plate. Similar peak errors were identified in [21] for unstiffened panels. Close to the critical frequency, the average error reduces and tends back to a value around ±1.5 dB. Above coincidence, the error vanishes, see **Fig. 11**(b,c).

7. Conclusions

The radiation efficiency of stiffened plates has been studied numerically using an FE model and the Rayleigh integral. An extensive parametric study covered 120 different combinations of stiffened plates with different numbers of stiffeners, and varying bending stiffness of both stiffeners and plate, to cover relevant parameter ranges. Empirical corrections for the effect of stiffeners were determined from the numerical data to expand existing asymptotic formulae for the prediction of the radiation efficiency for application to stiffened plates in different frequency regions.

The radiation efficiency of stiffened plates differs from unstiffened panels; it depends on whether the plate is forced on a stiffener or within a bay, on the flexibility of the stiffeners and the plate, and the number of stiffeners. In the low-frequency monopole region, for bay excitation the radiation efficiency depends on the ratio of stiffener and plate flexibility. As this increases, the effective radiating surface gradually reduces to that of a single bay and the radiation efficiency reduces correspondingly. For stiffener excitation, the radiation efficiency follows that of the unstiffened panel, but in rather extreme cases of very thin plates with deep stiffeners it can be reduced. These trends are accounted for by an empirical correction derived from curve fitting through results for 120 different stiffened plate configurations. In the short-circuiting region, the radiation efficiency is increased in comparison with the unstiffened panel, regardless of the excitation position. On average it is well approximated by an unstiffened bay-sized panel with clamped boundary conditions. When the frequency approaches the critical frequency, the radiation efficiency tends to that of the simply supported bay-sized panel.

The error between the proposed engineering model and the numerical simulations over all 120 cases has a mean value of 0.3 dB with a standard deviation of

± 1.5 dB over all frequency bands, which can be justified by the reduced calculation time. In single one-third octave bands the mean value of the error lies between -2 and 3 dB. The standard deviation is largest in the short-circuiting region with variations up to ± 5 dB, while in the monopole region it reaches up to ± 1.5 dB. The error decreases near coincidence and vanishes above the critical frequency.

Appendix A - Maidanik's formulae for clamped panels

To approximate the clamped panel with Maidanik's formulae, it was initially suggested to multiply the result of the simply supported panel by a factor of 2 (+3 dB) below the critical frequency [1]. This was found inadequate over the whole frequency region in [21], and overpredicts the results in the monopole region and near the critical frequency. To adapt the Maidanik formulae to clamped panels, suitable corrections for the monopole and short-circuiting regions are proposed here. The Maidanik formulae for a simply supported panel, found in [22] and based upon [1, 3, 5], are given as

$$\sigma = \begin{cases} \dfrac{4f^2 S}{{c_0}^2} & \text{for } f < f_1, \\ \max\left(\dfrac{4\pi^2}{{c_0}^2 S}\dfrac{D}{\mu}, \dfrac{P}{4\pi^2 S f_c}\dfrac{(1-\alpha^2)\ln\left(\dfrac{1+\alpha}{1-\alpha}\right)+2\alpha}{(1-\alpha^2)^{3/2}}\right) & \text{for } f_1 < f < f_c, \\ 0.45\sqrt{\dfrac{P f_c}{c_0}}\left(\dfrac{b}{a}\right)^{1/4} & \text{for } f \approx f_c, \\ \left(1-\dfrac{f_c}{f}\right)^{-1/2} & \text{for } f > f_c, \end{cases} \tag{18a-d}$$

where S is the surface area, P is the perimeter, a the longer and b the shorter side length of the panel, f_1 the fundamental natural frequency and $\alpha = \sqrt{f/f_c}$. In the short-circuiting region $(f_1 < f < f_c)$, the first part approximates the corner mode region and the second the edge mode region. The value around the coincidence region, where $f \approx f_c$, is used to limit the radiation efficiency. These formulae are normally used in an average sense with a one-third octave band resolution.

A.1 Monopole region

In the monopole region, where $f < f_1$, a reduction of radiation efficiency was found with clamped edges [21]. Due to the increased constraint, the effective radiating surface area of the monopole reduces. An equivalent radiating surface area S_{eq} of the clamped panel can be obtained by comparison with the simply supported panel. To calculate S_{eq}, the fundamental mode shapes have been numerically integrated over the panel surface. The ratio of their squares, which is proportional to the ratio of sound powers, gives $S_{eq} \approx 3/4\, S$, and this is substituted into Eq. (18a). Thus, a more general approximation of the radiation efficiency of an unstiffened panel is

$$\sigma = \frac{\varepsilon f^2 S}{{c_0}^2}, \tag{19}$$

where simply supported edges have $\varepsilon = 4$ and clamped edges $\varepsilon = 3$.

A.2 Short-circuiting region

In the corner mode region, the radiation efficiency is well approximated by Maidanik's suggested factor of 2 (+3 dB) but this needs correction when approaching the critical frequency in the edge mode region. This is addressed here in a simplified way. Instead of the additional +3 dB, the increase is reduced by 1 dB per one-third octave band in the two frequency bands immediately below the critical frequency. The corrected radiation efficiency in the short-circuiting region $f_1 < f < f_c$ can thus be written as

$$\sigma = \max\left(\frac{8\pi^2}{{c_0}^2 S}\frac{D}{\mu}, \frac{XP}{4\pi^2 S f_c}\frac{(1-\alpha^2)\ln\left(\frac{1+\alpha}{1-\alpha}\right)+2\alpha}{(1-\alpha^2)^{3/2}}\right), \tag{20}$$

where X corresponds to a factor of 2 (+3 dB) well below the critical frequency ($f \ll f_c$), but closer to the critical frequency is reduced by 1 dB per band. It is given by

$$X = \begin{cases} 10^{3/10} & \text{for } f \leq 10^{(n_{f_c}-3)/10} \\ 10^{2/10} & \text{for } f = 10^{(n_{f_c}-2)/10} \\ 10^{1/10} & \text{for } f = 10^{(n_{f_c}-1)/10} \\ 1 & \text{for } f \geq 10^{n_{f_c}/10} \end{cases}, \tag{21}$$

where n_{f_c} is the band number of the one-third octave band that includes the critical frequency.

In **Fig. 12** the numerical results obtained for the simply supported and clamped unstiffened panels with 3 mm thickness are compared with the Maidanik formulae in Eq. (18a-d) for the simply supported panel and the clamped panel by using the corrections proposed above. It shows that the monopole region is well approximated with $\varepsilon = 3$, to correct the radiating surface area of the clamped panel. In the short-circuiting region, the factor of 2 with the additional roll-off below the critical frequency captures the radiation efficiency of the clamped panel on average very well. Results for different panel thicknesses gave similar agreement.

ACKNOWLEDGMENT

The authors are grateful for the helpful suggestions of Dr Dong Zhao. We acknowledge the use of the IRIDIS High Performance Computing Facility, and associated support services at the University of Southampton, in the completion of this work.

REFERENCES

[1] G. Maidanik, 1962, "Response of Ribbed Panels to Reverberant Acoustic Fields," The Journal of the Acoustical Society of America, vol. 34, no. 6, pp. 809-826, doi: https://doi.org/10.1121/1.1918200.

[2] F. J. Fahy and P. Gardonio, 2007, Sound and structural vibration: radiation transmission and response (2nd Edition), Academic Press, London.

[3] C. E. Wallace, 1972, "Radiation Resistance of a Rectangular Panel," Journal of the Acoustical Society of America, vol. 51, no. 3B, pp. 946-952, doi: https://doi.org/10.1121/1.1912943.

[4] J. W. Strutt (Baron Rayleigh), 1945, The theory of sound (2nd Edition), Dover, New York.

[5] F. G. Leppington, E. G. Broadbent, and K. H. Heron, 1982, "The acoustic radiation efficiency of rectangular panels," Proceedings of the Royal Society of London. Series A: Mathematical, Physical and Engineering Sciences, vol. 382, no. 1783, doi: https://doi.org/10.1098/rspa.1982.0100.

[6] G. Xie, D. J. Thompson, and C. J. C. Jones, 2005, "The radiation efficiency of baffled plates and strips," Journal of Sound and Vibration, vol. 280, no. 1-2, pp. 181-209, doi: https://doi.org/10.1016/J.JSV.2003.12.025.

[7] D. M. Egle and J. L. Sewall, 1968, "An analysis of free vibration of orthogonally stiffened cylindrical shells with stiffeners treated as discrete elements," AIAA Journal, vol. 6, no. 3, pp. 518-526, doi: https://doi.org/10.2514/3.4528.

[8] L. Dozio and M. Ricciardi, 2009, "Free vibration analysis of ribbed plates by a combined analytical–numerical method," Journal of Sound and Vibration, vol. 319, no. 1-2, pp. 681-697, doi: https://doi.org/10.1016/J.JSV.2008.06.024.

[9] K. Zhang, J. Pan, and T. R. Lin, 2021, "Vibration of rectangular plates stiffened by orthogonal beams," Journal of Sound and Vibration, vol. 513, p. 116424, doi: https://doi.org/10.1016/j.jsv.2021.116424.

[10] M. Heckl, 1961, "Wave Propagation on Beam-Plate Systems," Journal of the Acoustical Society of America, vol. 33, no. 5, pp. 640-651, doi: https://doi.org/10.1121/1.1908750.

[11] Y. Du, D. Jia, H. Li, C. Gao, and H. Wang, 2022, "A unified method to analyze free and forced vibration of stiffened plates under various edge conditions," European

Journal of Mechanics - A/Solids, vol. 94, p. 104573, doi: https://doi.org/10.1016/j.euromechsol.2022.104573.

[12] M. Heckl, 1964, "Investigations on the Vibrations of Grillages and Other Simple Beam Structures," The Journal of the Acoustical Society of America, vol. 36, no. 7, pp. 1335-1343, doi: https://doi.org/10.1121/1.1919206.

[13] B. R. Mace, 1980, "Periodically stiffened fluid-loaded plates, I: Response to convected harmonic pressure and free wave propagation," Journal of Sound and Vibration, vol. 73, no. 4, pp. 473-486, doi: https://doi.org/10.1016/0022-460X(80)90662-8.

[14] B. R. Mace, 1980, "Periodically stiffened fluid-loaded plates, II: Response to line and point forces," Journal of Sound and Vibration, vol. 73, no. 4, pp. 487-504, doi: https://doi.org/10.1016/0022-460X(80)90663-X.

[15] B. R. Mace, 1981, "Sound radiation from fluid loaded orthogonally stiffened plates," Journal of Sound and Vibration, vol. 79, no. 3, pp. 439-452, doi: https://doi.org/10.1016/0022-460X(81)90321-7.

[16] D. J. Mead, 1990, "Plates with regular stiffening in acoustic media: Vibration and radiation," Journal of the Acoustical Society of America, vol. 88, no. 1, pp. 391-401, doi: https://doi.org/10.1121/1.399915.

[17] M. D. Olson and C. R. Hazell, 1977, "Vibration studies on some integral rib-stiffened plates," Journal of Sound and Vibration, vol. 50, no. 1, pp. 43-61, doi: https://doi.org/10.1016/0022-460X(77)90550-8.

[18] E. Reynders, C. Van Hoorickx, and A. Dijckmans, 2016, "Sound transmission through finite rib-stiffened and orthotropic plates," Acta Acustica united with Acustica, vol. 102, no. 6, pp. 999-1010, doi: https://doi.org/10.3813/AAA.919015.

[19] J.-M. Mencik and M.-L. Gobert, 2012, "Wave Finite Element based Strategies for Computing the Acoustic Radiation of Stiffened or Non-Stiffened Rectangular Plates subject to Arbitrary Boundary Conditions", in *Proceedings of the Eleventh International Conference on Computational Structures Technology*, B.H.V. Topping, (Editor), Civil-Comp Press, Stirlingshire, paper 218. doi: https://doi.org/10.4203/ccp.99.218

[20] P. Langer, M. Maeder, C. Guist, M. Krause, and S. Marburg, 2017, "More Than Six Elements per Wavelength: The Practical Use of Structural Finite Element Models and Their Accuracy in Comparison with Experimental Results," Journal of Computational Acoustics, vol. 25, no. 4, doi: https://doi.org/10.1142/S0218396X17500254.

[21] G. Squicciarini, D. J. Thompson, and R. Corradi, 2014, "The effect of different combinations of boundary conditions on the average radiation efficiency of rectangular plates," Journal of Sound and Vibration, vol. 333, no. 17, pp. 3931-3948, doi: https://doi.org/10.1016/J.JSV.2014.04.022.

[22] F. J. Fahy and D. J. Thompson, 2015, Fundamentals of Sound and Vibration (2nd Edition), CRC Press, London.

Table caption list

Table 1	Parameters used in the FE model and Rayleigh integral for numerical calculations
Table 2	Change of radiation efficiency, relative to the unstiffened panel (σ_0), for bay excitation in the monopole region (10 Hz) and the short-circuiting region (2 kHz). Also listed is the ratio of bay-to-plate surface areas expressed in decibels

Figure caption list

Fig. 1	Finite element model of a stiffened plate with a zoomed view of the sampling grid (dots) and the FE mesh adopted in the calculations
Fig. 2	Coordinate system used to evaluate the Rayleigh integral for a baffled plate divided into small elemental sound sources of area ΔS_i
Fig. 3	Stiffened plate configurations of Cases 1-4 with the 20 excitation positions; ○, bay positions; ×, stiffener positions
Fig. 4	Radiation efficiency of the stiffened plate Case 3 compared with the unstiffened panel; —, bay-excited stiffened plate; – – –, stiffener-excited stiffened plate;· · · ·, unstiffened clamped panel; – · –, unstiffened clamped bay-sized panel
Fig. 5	Radiation efficiency of the stiffened plate Cases 1-4 compared to the unstiffened panel for (a) bay and (b) stiffener excitation; ▬, unstiffened panel; —, Case 1; · · · ·, Case 2; – – –, Case 3; – · –, Case 4
Fig. 6	Radiation efficiency of Case 3 with a plate thickness of (a) $h = 3.0$ mm, and (b) $h = 6.0$ mm and a stiffener depth of 40 mm compared to an unstiffened panel of the same thickness; —, bay-excited stiffened plate; – – –, stiffener-excited stiffened plate; · · · ·, unstiffened clamped panel
Fig. 7	Radiation efficiency over frequency of Case 3 with a plate thickness of 3 mm and varying stiffener depth compared to the unstiffened panel for (a) bay excitation and (b) stiffener excitation; ▬, unstiffened panel; —, $h_s = 20$ mm; · · · ·, $h_s = 40$ mm; – – –, $h_s = 60$ mm; – · –, $h_s = 100$ mm
Fig. 8	Change of radiation efficiency in the monopole region plotted against the ratio of stiffener to plate bending stiffness for varying stiffener depth (20, 40, 60, 80, 100 mm) and plate thickness (1.5, 3.0, 6.0 mm); black, bay excitation; grey, stiffener excitation; ×, Case 1; ○, Case 4
Fig. 9	Non-dimensional change in radiation efficiency in the monopole region plotted against the non-dimensional ratio of stiffener and plate bending stiffness for Cases 1-4 with varying plate thickness and stiffener depth for (a) bay excitation and (b) stiffener excitation; ○, $h = 1.5$ mm; □, $h = 3$ mm; Δ, $h = 6$ mm; ▬, fitted asymptotic function γ_{fit}; – – –, limiting values between the different regions
Fig. 10	Radiation efficiency of stiffened plates excited in the bay with different boundary conditions and values of β, (a) $\beta = -0.47$ and (b) $\beta = 1.28$; ▬, clamped stiffened plate; ▪ ▪ ▪, simply supported stiffened plate; —, simply supported bay-sized panel with Eq. (18a-d); · · · ·, clamped bay-sized panel with Eq. (18a-d) and the corrections from Eqs. (19) and (20)

Fig. 11	Differences of the predictions based on Eq. (17a-d) compared with the numerical results (FE model with Rayleigh integral) for (a) 1.5 mm, (b) 3 mm, and (c) 6 mm plate thickness; □, mean value (bay excitation); —, error bars (bay excitation), +/- one standard deviation range; ●, mean value (stiffener excitation); · · · ·, error bars (stiffener excitation), +/- one standard deviation range;– – –, minimum and maximum difference
Fig. 12	Radiation efficiency of an unstiffened panel of 3 mm thickness; ▬, clamped edges; - - -, simply supported edges; —, simply supported approximated with Eq. (18a-d); · · · ·, clamped approximated with Eq. (18a-d) and the corrections from Eqs. (19) and (20)

Tables

Table 1 Parameters used in the FE model and Rayleigh integral for numerical calculations

Symbol	Variable	Value
a	Plate length (x-axis)	0.8 m
b	Plate width (y-axis)	0.6 m
h	Plate thickness	1.5, 3 and 6 mm
w_s	Stiffener width	20 mm
h_s	Stiffener depth	10, 20, …, 100 mm
t_s	Stiffener thickness (flange & web)	3 mm
E	Young's modulus	71 GPa
ρ	Density	2700 kg/m^3
ν	Poisson's ratio	0.3
η	Damping loss factor	0.01
ρ_0	Density of air	1.21 kg/m^3
c_0	Speed of sound in air	343 m/s

Table 2 Change of radiation efficiency, relative to the unstiffened panel (σ_0), for bay excitation in the monopole region (10 Hz) and the short-circuiting region (2 kHz). Also listed is the ratio of bay-to-plate surface areas expressed in decibels

	Case 1	Case 2	Case 3	Case 4
$10\log_{10}(S_{\mathrm{bay}}/S)$	−6.1 dB	−7.8 dB	−9.3 dB	−10.3 dB
$10\log_{10}(\sigma/\sigma_0)$ at 10 Hz	−6.6 dB	−8.0 dB	−9.1 dB	−9.8 dB
$10\log_{10}(\sigma/\sigma_0)$ at 2 kHz	3.0 dB	3.6 dB	5.4 dB	6.4 dB

Figures

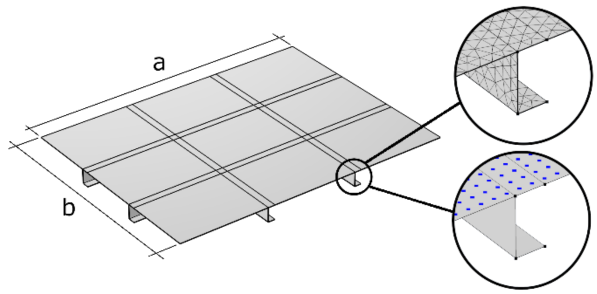

Fig. 1 Finite element model of a stiffened plate with a zoomed view of the FE mesh and the sampling grid (dots) adopted in the calculations

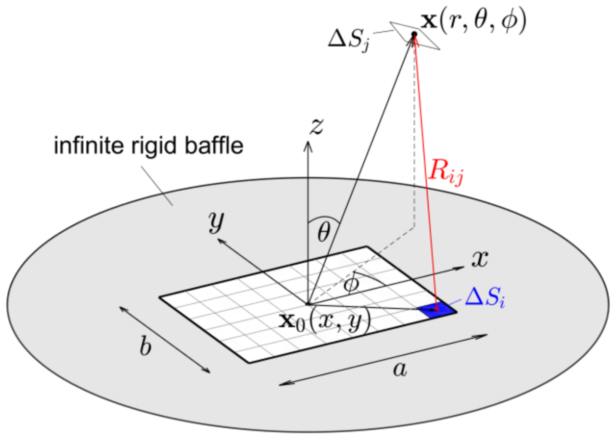

Fig. 2 Coordinate system used to evaluate the Rayleigh integral for a baffled plate divided into small elemental sound sources of area ΔS_i

701

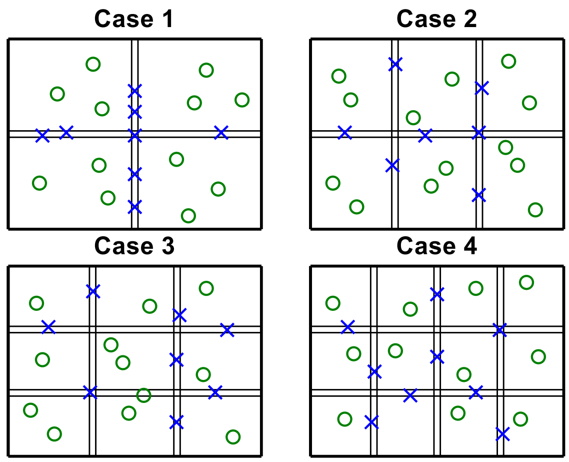

Fig. 3 Stiffened plate configurations of Cases 1-4 with the 20 excitation positions; ○, bay positions; ×, stiffener positions

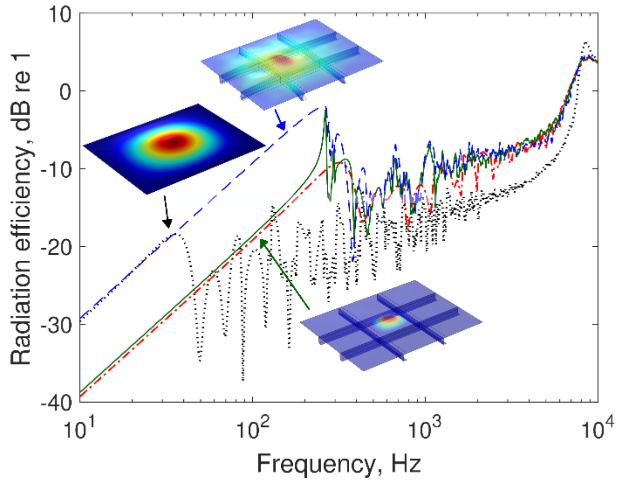

Fig. 4 Radiation efficiency of the stiffened plate Case 3 compared with the unstiffened panel; —, bay-excited stiffened plate; – – –, stiffener-excited stiffened plate;· · · ·, unstiffened clamped panel; – · –, unstiffened clamped bay-sized panel

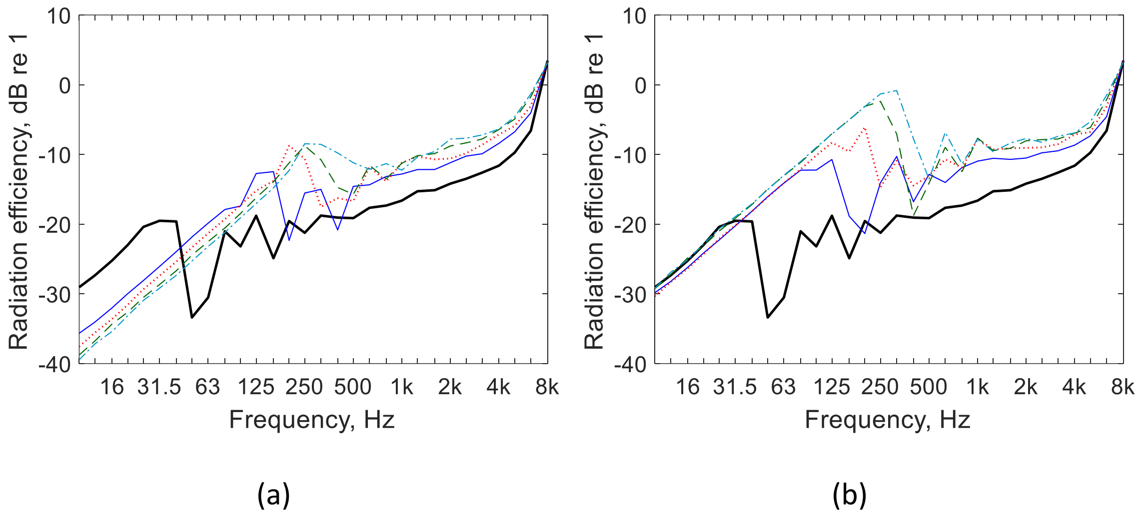

Fig. 5 Radiation efficiency of the stiffened plate Cases 1-4 compared to the unstiffened panel for (a) bay and (b) stiffener excitation; ▬, unstiffened panel; —, Case 1; · · · ·, Case 2; – – –, Case 3; –·–, Case 4

704

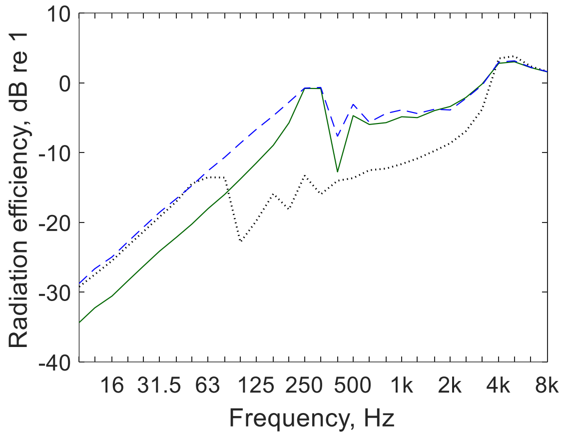

(a)

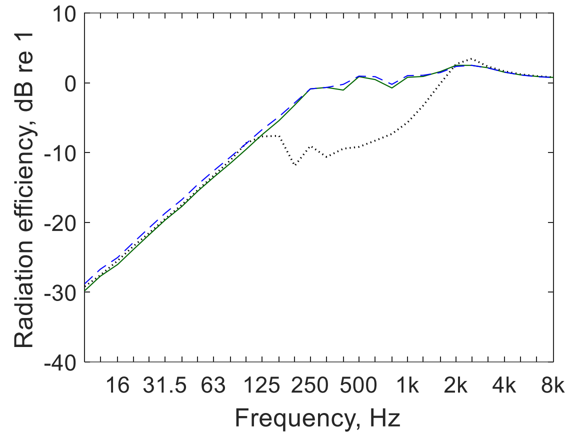

(b)

Fig. 6 Radiation efficiency of Case 3 with a plate thickness of (a) $h = 3.0$ mm, and (b) $h = 6.0$ mm and a stiffener depth of 40 mm compared to an unstiffened panel of the same thickness; —, bay-excited stiffened plate; – – –, stiffener-excited stiffened plate; · · · ·, unstiffened clamped panel

705

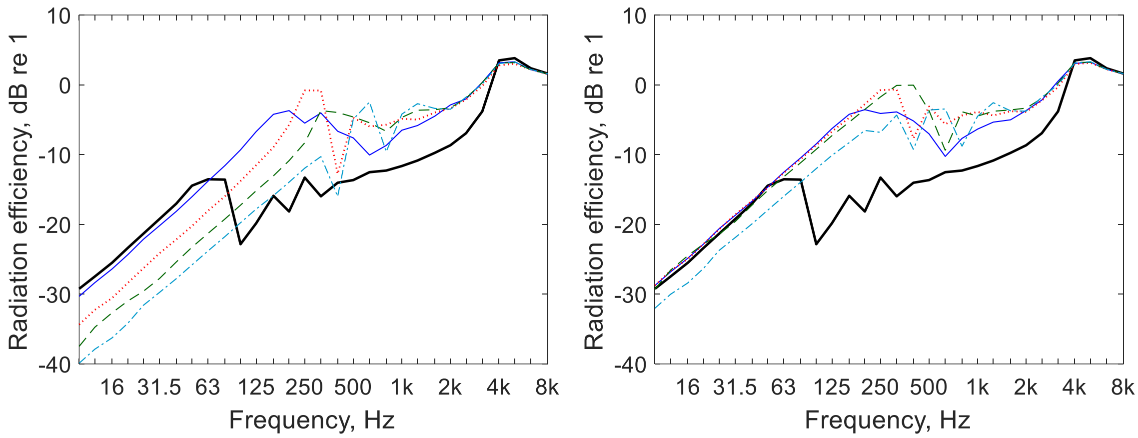

(a) (b)

Fig. 7 Radiation efficiency over frequency of Case 3 with a plate thickness of 3 mm and varying stiffener depth compared to the unstiffened panel for (a) bay excitation and (b) stiffener excitation; ▬, unstiffened panel; —, $h_s = 20$ mm; · · · ·, $h_s = 40$ mm; – – –, $h_s = 60$ mm; – · –, 100 mm

706

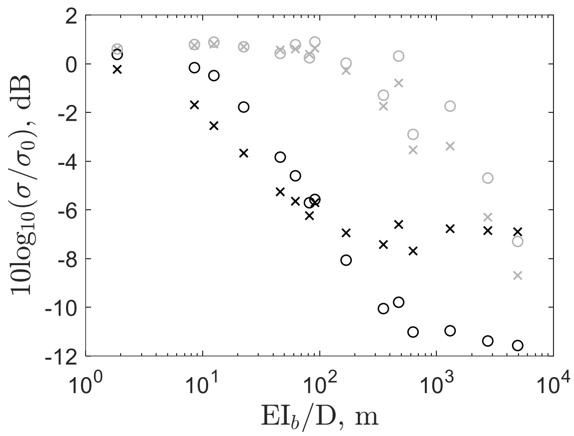

Fig. 8 Change of radiation efficiency in the monopole region plotted against the ratio of stiffener to plate bending stiffness for varying stiffener depth (20, 40, 60, 80, 100 mm) and plate thickness (1.5, 3.0, 6.0 mm); black, bay excitation; grey, stiffener excitation; ×, Case 1; O, Case 4

707

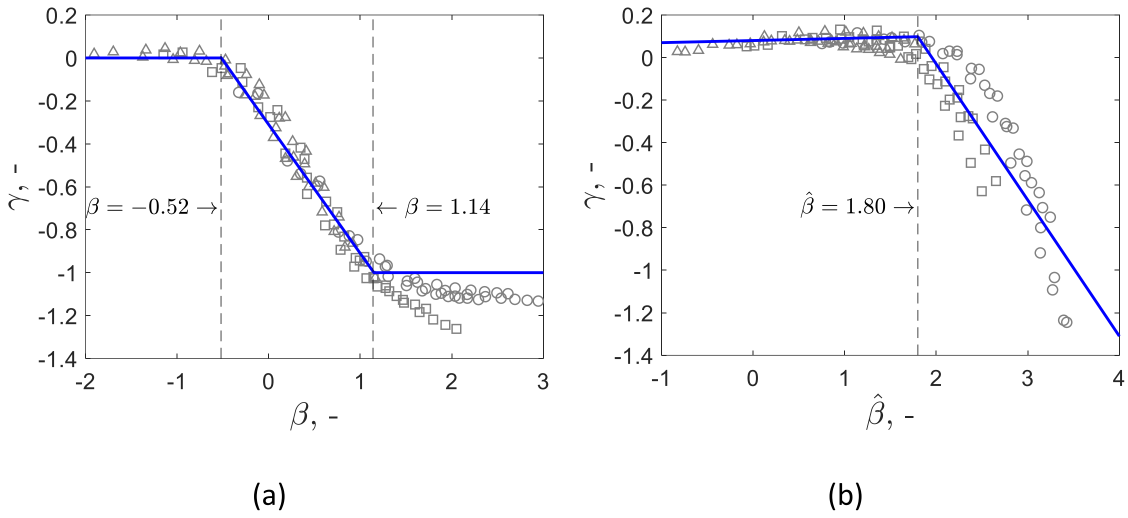

Fig. 9 Non-dimensional change in radiation efficiency in the monopole region plotted against the non-dimensional ratio of stiffener and plate bending stiffness for Cases 1-4 with varying plate thickness and stiffener depth for (a) bay excitation and (b) stiffener excitation; ○, $h = 1.5$ mm; □, $h = 3$ mm; Δ, $h = 6$ mm; ▬, fitted asymptotic function γ_{fit}; – – –, limiting values between the different regions

708

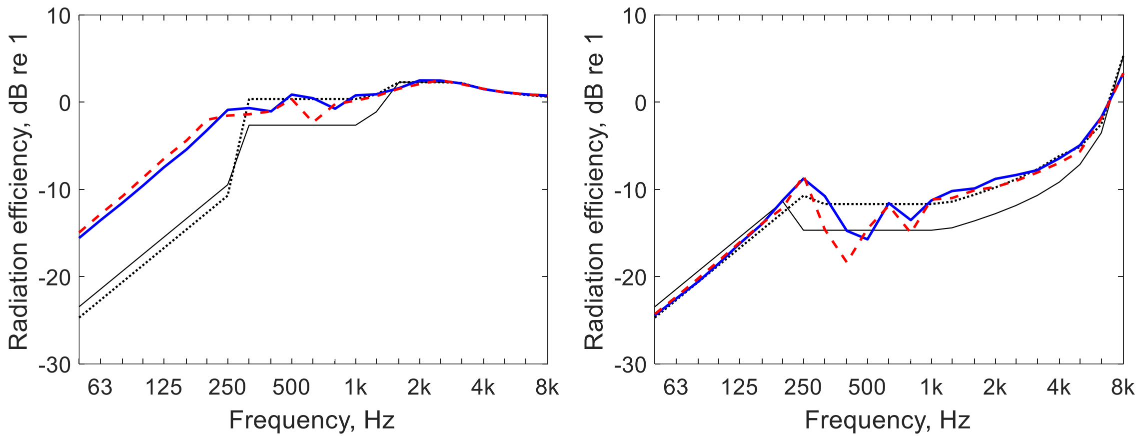

(a) (b)

Fig. 10 Radiation efficiency of stiffened plates excited in the bay with different boundary conditions and values of β, (a) $\beta = -0.47$ and (b) $\beta = 1.28$; ▬, clamped stiffened plate; - - -, simply supported stiffened plate; —, simply supported bay-sized panel with Eq. (18a-d); $\cdot\cdot\cdot\cdot$, clamped bay-sized panel with Eq. (18a-d) and the corrections from Eqs. (19) and (20)

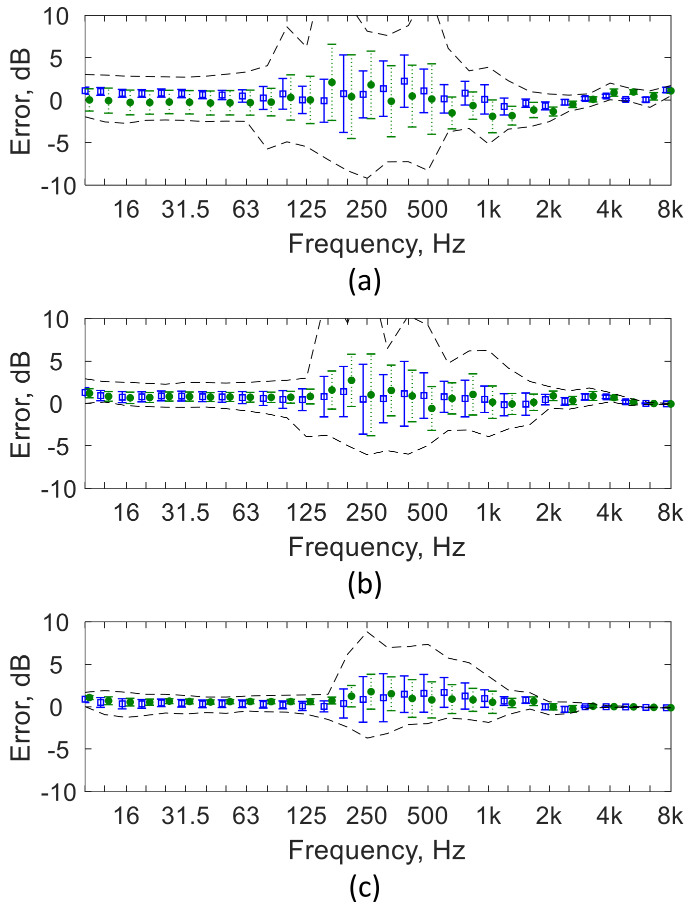

Fig. 11 Differences of the predictions based on Eq. (17a-d) compared with the numerical results (FE model with Rayleigh integral) for (a) 1.5 mm, (b) 3 mm, and (c) 6 mm plate thickness; □, mean value (bay excitation); —, error bars (bay excitation), +/- one standard deviation range; ●, mean value (stiffener excitation); · · · ·, error bars (stiffener excitation), +/- one standard deviation range;– – –, minimum and maximum difference

710

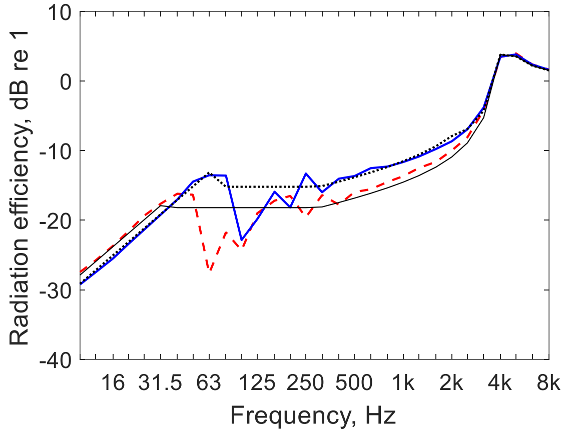

Fig. 12 Radiation efficiency of an unstiffened panel of 3 mm thickness; ▬, clamped edges; - - -, simply supported edges; —, simply supported approximated with Eq. (18a-d); · · · ·, clamped approximated with Eq. (18a-d) and the corrections from Eqs. (19) and (20)